

Parametric and Nonparametric Identification and Robust Control of a Rotational/Translational Actuator

M. Tavakoli[†], H. D. Taghirad^{*} and M. Abrishamchian^{*}

[†] Department of Electrical and Computer Engineering
University of Western Ontario, Canada
E-mail: tavakoli@uwo.ca

^{*} Department of Electrical Engineering
K. N. Toosi University of Technology, Iran

Abstract—RTAC¹ benchmark problem considers a nonlinear fourth-order dynamical system involving the nonlinear interaction of a translational oscillator and an eccentric rotational proof mass. This problem has been posed to investigate the utility of a rotational proof mass actuator for stabilizing translational motion. In order to implement any of the model-based controllers proposed in the literature, the values of model parameters are required which are generally difficult to determine rigorously. In this paper, an approach to the least-squares estimation of system parameters is discussed and practically applied to the benchmark problem. Next, in order to design an H_∞ controller, the nonlinear system is modelled as a perturbed linear system using an effective identification scheme. Experimental results confirm that this approach can effectively condense the whole nonlinearities, uncertainties, and disturbances within the system into a favorable perturbation block. Finally, an effective mixed-sensitivity problem is developed for the system to satisfy all performance requirements as well as robust stability despite actuator saturation.

I. INTRODUCTION

The RTAC experiment has originally been studied as a simplified model of a dual-spin spacecraft to investigate the resonance capture phenomenon [1]. It is shown that this system is *mathematically* and *qualitatively* equivalent to a dual-spin spacecraft, i.e., they have similar averaged equations and exhibit similar dynamic behaviors.

The RTAC system has been studied later to investigate the usefulness of a rotational proof mass actuator for stabilizing translational motion [2]. In this nonlinear system, unlike a linear proof mass actuator, the actuator stroke limitations are implicitly involved in the system dynamics [3].

Consider the translational oscillator with an eccentric rotational proof mass actuator shown in Figure 1. The oscillator consists of a cart of mass M connected to a fixed wall by a linear spring of stiffness k . The motion is confined in one direction and is merely in the horizontal plane, so that gravitational forces do not contribute. The proof mass actuator attached to the cart has mass m and moment of inertia I about its center of mass, which is located at a distance e from the point about which the proof mass rotates. N denotes the control torque applied to the

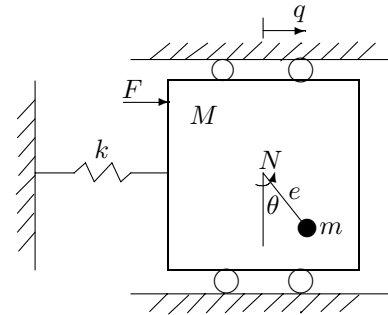


Fig. 1. Rotational actuator to control a translational oscillator

proof mass, and F is the disturbance force on the cart. The control objective is the oscillator stabilization despite external disturbances via the control torque provided by the rotational proof-mass actuator.

In this nonlinear benchmark problem, it is required to design a controller such that:

- a) The closed-loop system is stable.
- b) The closed-loop system exhibits good settling behavior for a class of initial conditions.
- c) The closed-loop system exhibits good disturbance rejection compared to the uncontrolled oscillator for a class of disturbance signals.
- d) The control effort is feasible.

A number of research work are reported on this problem. For instance, Bupp, Bernstein and Coppola implement four nonlinear controllers on the RTAC, including an integrator back-stepping controller and three passivity-based controllers [4]. Haddad and Chellaboina apply their method of designing nonlinear fixed-order dynamic passive controllers for passive systems to the RTAC system [5]. Dussey and El-Ghaoui develop a measurement-scheduled output-feedback controller with an LMI approach for the system [6].

II. SYSTEM MODELLING

Let q and \dot{q} denote the translational position and velocity of the cart, and let θ and $\dot{\theta}$ denote the angular position and velocity of the rotational proof mass (Figure 1). The equations of motion for the system are given as:

$$(M + m)\ddot{q} + kq = -me(\ddot{\theta} \cos \theta - \dot{\theta}^2 \sin \theta) + F, \quad (1)$$

$$(I + me^2)\ddot{\theta} = -me\dot{q} \cos \theta + N. \quad (2)$$

¹Rotational/Translational Actuator

With some transformations [2], the nondimensionalized state equations of the system are given by

$$\dot{\mathbf{x}} = \mathbf{f}(\mathbf{x}) + \mathbf{g}(\mathbf{x})u + \mathbf{d}(\mathbf{x})w,$$

where,

$$\begin{aligned} \mathbf{f}(\mathbf{x}) &= \left(x_2 \quad \frac{-x_1 + \epsilon x_4^2 \sin x_3}{1 - \epsilon^2 \cos^2 x_3} \quad x_4 \quad \frac{\epsilon \cos x_3 (x_1 - \epsilon x_4^2 \sin x_3)}{1 - \epsilon^2 \cos^2 x_3} \right)^T, \\ \mathbf{g}(\mathbf{x}) &= (0 \quad -\epsilon \cos x_3 \quad 0 \quad 1)^T / (1 - \epsilon^2 \cos^2 x_3), \\ \mathbf{d}(\mathbf{x}) &= (0 \quad 1 \quad 0 \quad -\epsilon \cos x_3)^T / (1 - \epsilon^2 \cos^2 x_3). \end{aligned}$$

Here, $\mathbf{x} = (x_1 \quad x_2 \quad x_3 \quad x_4)^T = (\xi \quad \dot{\xi} \quad \theta \quad \dot{\theta})^T$, where ξ is the normalized cart position, and u and w represent the normalized control torque and disturbance, respectively. The parameter $\epsilon = me / \sqrt{(I + me^2)(M + m)}$ represents the coupling between the translational and rotational motions.

The air friction and spring damping can be considered as disturbances on the cart, and may be modelled as viscous frictions with coefficients b and c , respectively. Therefore, (1) becomes

$$(M + m)\ddot{q} + kq + b\dot{q} = -me(\ddot{\theta} \cos \theta - \dot{\theta}^2 \sin \theta) - c\dot{q}.$$

The equilibrium point is $\mathbf{x}_e = (0 \quad 0 \quad \theta_0 \quad 0)^T$ and $u_e = 0$, where θ_0 is any arbitrary value, provided the disturbance w is zero. Using Jacobians for this equilibrium point, the transfer function from the normalized torque u to the normalized cart position ξ is found to be

$$\frac{\Xi(s)}{U(s)} = \frac{\epsilon \cos \theta_0}{(\epsilon^2 \cos^2 \theta_0 - 1)s^2 - \frac{v}{\sqrt{k(M+m)}}s - 1} \quad (3)$$

where $v = b + c$. This transfer function has a varying DC gain, however, its modes are fairly insensitive to the variations of θ_0 . The term $\cos \theta_0$ in the numerator implies that the pendulum vibrations about $\theta = 0$ have the most influence on the cart displacement, while at $\theta = 90^\circ$ they have the least effect.

III. EXPERIMENTAL TESTBED

The experimental testbed, aimed to realize the model depicted in Figure 1, is constructed (Figure 2). The basis for this setup is provided by an aluminum plate onto which five steel bars are perpendicularly mounted. Using an upper plate, a rigid ceiling is provided for the setup. The spring is realized by means of two beams fastened to the ceiling. These beams also serve to suspend the cart made of acrylic plates in the air, in order to reduce the friction as much as possible. Due to the setup rigidity, the cart motion is merely confined to one direction, and roll, yaw and pitch movements are suppressed as well. A DC motor and a tachometer are centered on the lower and upper plates of the cart, with their shafts secured together through a coupling to avoid eccentricity. The same coupling also serves to hold the eccentric arm.

The control torque is provided by the DC motor. A PWM current drive controls, through a PI feedback loop, the torque applied by the motor on the eccentric arm. The angular position of the arm is determined by integrating

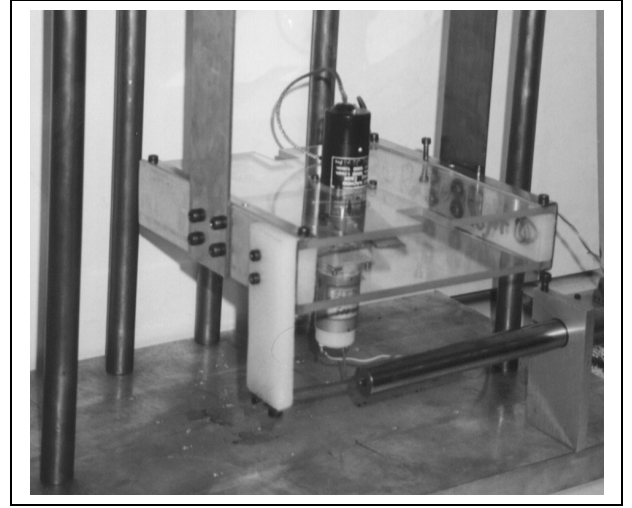


Fig. 2. The RTAC setup

the angular velocity readings from the tachometer. In order to determine the cart translational position, a linear variable differential transformer (LVDT) is utilized. It consists of a body which is mounted on the basis, and a core which is attached to the cart and travels within the body. Therefore, the cart travels are translated to a proportional voltage at the output terminals of the LVDT.

IV. PARAMETRIC IDENTIFICATION

For any model-based control such as [1], [2], [4], [5] and [6], it is necessary to have the values of system parameters. While rigorous determination of the parameters of the actual system is quite difficult, it is possible to estimate them using the least-squares method. To do so, the system equations of motion are viewed as a set of equations which are unknown in system parameters and in which certain functions of measurements serve as regressors. Next, a consistency measure may be defined as the ratio of standard deviation of the estimates to their mean value. If this measure is less than 30%, then the model based on the mean values should be in well agreement with the actual system. More consistent parameter estimates will be found if one or more of the parameters can be estimated separately, rather than all of them being estimated at one attempt.

The first equation of motion of the RTAC system can be written as

$$\frac{M + m}{k}\ddot{q} + \frac{v}{k}\dot{q} + \frac{d}{k}\text{sgn}(\dot{q}) + \frac{me}{k}(\ddot{\theta} \cos \theta - \dot{\theta}^2 \sin \theta) = -q,$$

where v is due to the air friction and spring damping, and d is the Coulomb friction coefficient. In a free-oscillation experiment in which the motor is idle and the cart is subject to free oscillations due to its initial position, the term $\ddot{\theta} \cos \theta - \dot{\theta}^2 \sin \theta$ will be negligible. Therefore, at the i -th sampling time during an identification experiment:

$$\begin{aligned} \Phi_i \Theta &= -q_i, \\ \Phi_i &= (\ddot{q}_i \quad \dot{q}_i \quad \text{sgn}(\dot{q}_i)), \\ \Theta &= \left(\frac{M+m}{k} \quad \frac{v}{k} \quad \frac{d}{k} \right)^T. \end{aligned}$$

Here, the vector of regressed variables Θ can be estimated in the sense of least squares if we have measurements leading to the values of the regressor matrix $\Phi = (\Phi_1 \ \cdots \ \Phi_n)^T$ and the observation vector $Q = (-q_1 \ \cdots \ -q_n)^T$:

$$\Theta = (\Phi^T \Phi)^{-1} \Phi^T Q.$$

To find Φ and Q , the cart position data are logged and then filtered by a 9th-order Chebychev filter implemented using a zero-phase-distortion routine (Matlab function *filtfilt*) to remove the measurement noise. The filtered cart position data are then differentiated to find \dot{q} and \ddot{q} . The least-squares results obtained using ten free-oscillation experiments for different cart initial positions are listed in Table 1a. Weighing the acrylic plates, motor, tachometer and arm results in $M + m = 1.230$ Kg, and therefore $k = 132.6$ N/m, $v = 0.5543$ and $d = 24 \times 10^{-3}$.

The same scheme is used to find the rest of system parameters through a set of forced-oscillation experiments. Taking into account the rotational viscous friction in the second equation of motion, the two equations can be rewritten as

$$\begin{aligned} me(\ddot{\theta} \cos \theta - \dot{\theta}^2 \sin \theta) &= -kq - (M + m)\ddot{q} - v\dot{q} - d\text{sgn}(\dot{q}), \\ me\dot{q} \cos \theta - K_m i + \\ K_{v1} u_{\dot{\theta}} \dot{\theta} + K_{v2} u_{-\dot{\theta}} \dot{\theta} &= -(I + me^2)\ddot{\theta}. \end{aligned}$$

where i is the motor current, K_m is the motor torque constant, and K_{v1} and K_{v2} represent the coefficients of asymmetric viscous friction in the arm rotational motion. For the setup built in the laboratory, $I + me^2$ is mathematically determined to be 4.78×10^{-5} . Having obtained the estimates of $M + m$, k , v and d previously, this set of equations can simultaneously be solved with respect to the parameters me , K_m , K_{v1} and K_{v2} . Twenty forced-oscillation experiments with different cart initial positions and arm initial angles are performed while the input amplitudes are swept from 50% to 100% of their maximum value. The estimates are listed in Table 1b. Small consistency measures for the parameters estimated through free- and force-oscillation experiments promise a good match between the estimated mathematical model and the actual system. Estimated values of important system parameters are summarized in Table 1c.

Table 1. From top to bottom: Least square results of (a) free-oscillation experiments, (b) forced-oscillation experiments and (c) RTAC system parameter estimates

	$\frac{M+m}{k}$	$\frac{v}{k}$	$\frac{d}{k}$
Mean	9.27×10^{-3}	4.18×10^{-3}	1.81×10^{-4}
Std.dev.	0.64 %	9.68 %	14.74 %
Mean			

	me	K_m	K_{v1}	K_{v2}
Mean	1.06×10^{-3}	4.02×10^{-2}	1.39×10^{-4}	1.49×10^{-4}
Std.dev.	15.5 %	6.2 %	34 %	33 %
Mean				

Total mass	$M + m$	1.23 kg
Arm inertia moment	$I + me^2$	950 gcm ²
Spring stiffness	k	132.6 N/m
Coupling parameter	ϵ	0.1
Torque constant	K_m	0.08 N.m./A

V. NONPARAMETRIC IDENTIFICATION AND ROBUST CONTROL

The RTAC problem was originally posed as a nonlinear benchmark problem, and consequently all the previous researches have relied on the ideal non-dissipative model of the nonlinear system given by Equations (1) and (2). However, this approach cannot take into account, e.g. unmodelled dynamics and/or deviations from this nonlinear model which do exist in practice. On the other hand, the control objectives such as internal stability, fast settling, and good disturbance rejection in spite of limited control effort are well suited to linear robust control synthesis. We design a linear H_∞ controller while the nonlinear system is estimated as a nominal linear system in addition to uncertainty.

A nonlinear system can be modelled as an unstructured set \mathcal{P} of linear plants. In other words, a nominal model $P_0(s)$, a weight $W(s)$, and a stable perturbation Δ satisfying $\|\Delta\|_\infty \leq 1$ may be found in such a way that the frequency response of the nonlinear system is represented as $P(s) = (1 + \Delta(s)W(s))P_0(s)$. Since $\|\Delta\|_\infty \leq 1$, $W(j\omega)$ provides the uncertainty profile at each frequency:

$$\left| \frac{P(j\omega)}{P_0(j\omega)} - 1 \right| \leq W(j\omega), \quad \forall \omega.$$

If a set of identification experiments is performed on the nonlinear system under different operating conditions, the resulting linear frequency response estimates $P(j\omega)$ will form the set \mathcal{P} . By finding a *nominal fit* $P_0(j\omega)$ through these frequency response estimates which reduces the variations among them to a minimum, the whole nonlinearities, disturbances and uncertainties of the system will be condensed into the perturbation ΔW . This provides enough information for an H_∞ synthesis.

To produce a series of linear frequency response estimates of the nonlinear system under different operating regimes, system identification based on prediction-error method is performed. In the prediction-error method [7], a least-squares minimization is used to determine the model parameter vector θ in such a way that the sum square of the prediction errors

$$\epsilon(t, \theta) = y(t) - \hat{y}(t|t-1; \theta), \quad t = 1, 2, \dots, N,$$

is minimized. The details of each step of this method as applied to RTAC is reported next.

A. Prediction-Error System Identification

First a simulation study is conducted on how to handle the varying DC gain of the transfer function in Equation (3). The DC gain which varies with the arm angle θ_0 can reduce the accuracy of the frequency response estimates, because for different operating conditions of the pendulum, the optimization will converge to different local minima. A well-conditioned solution to this problem is shown in Figure 3 where a hypothetical transfer function

²Perturbations other than multiplicative are also allowed.

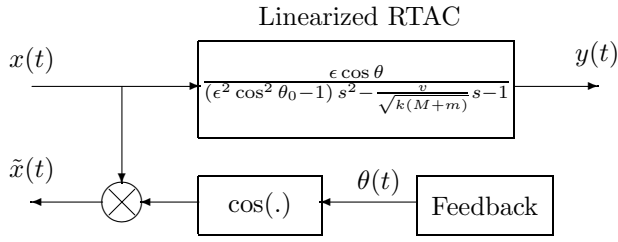


Fig. 3. Compensation of the varying DC gain

is found which only includes the time-invariant portion of transfer function (3):

$$\frac{y(t)}{\tilde{x}(t)} = \frac{\epsilon}{(\epsilon^2 \cos^2 \theta_0 - 1) s^2 - \frac{v}{\sqrt{k(M+m)}} s - 1}.$$

For identification tests, a concatenation of positive and negative multisines is used as the excitation input³. The reason is that a multisine signal demonstrates an almost flat spectrum over the frequency range of interest. It is also highly persistent excitation as the sum of n sinusoids is persisting of an order not less than $2n - 2$ [7]. Since the RTAC system is uncontrollable at $\theta_0 = \pm 90^\circ$, the excitation input is taken to be zero when $\cos \theta_0$ nears zero, e.g. when $|\cos \theta_0| \leq 0.05$. Within this uncontrollable span and in the absence of input, the arm momentum of inertia passes the arm through this region.

Identification tests are done for different initial arm angles such that the estimated transfer functions are valid representatives of the nonlinear system all over its operating range. The amplitudes of the multisine range from 50% to 100% of their maximum value. We initialize the prediction-error minimization with a parameter vector θ specifying the model structure of the linearized model (3).

The resultant frequency response estimates as well as the frequency response of the following selected nominal system are shown in Figure 4a:

$$P_0(s) = 3.7 \times 10^{-3} \times \frac{(s - 175.7)(s + 32.7)(s + 14.5 \pm j26.6)}{(s + 2.7 \pm j12.9)(s + 4.1 \pm j37.4)}.$$

While the magnitudes of the frequency response estimates experience two peaks at 12.9 rad/s and 37.4 rad/s, our simulation study had previously shown the first peak only. The reason is that the flexible beams used to realize the springs in the experimental setup form a spring-mass-spring-mass system which has one rigid and one flexible modes. The peak at 12.9 rad/s corresponds to the rigid mode of the mechanical structure, while the other harmonic represents the fundamental frequency of the flexible structure.

The uncertainty profile $\left| \frac{P(j\omega)}{P_0(j\omega)} - 1 \right|$ and the uncertainty weighting function

$$W(j\omega) = 0.55 \frac{\left(\frac{j\omega}{2} + 1\right)\left(\frac{j\omega}{80} + 1\right)}{\left(\frac{j\omega}{5} + 1\right)\left(\frac{j\omega}{1000} + 1\right)} \quad (4)$$

³Functions *msinclip* and *msinprep* in the Frequency Domain Identification Toolbox (FDIDENT) [8].

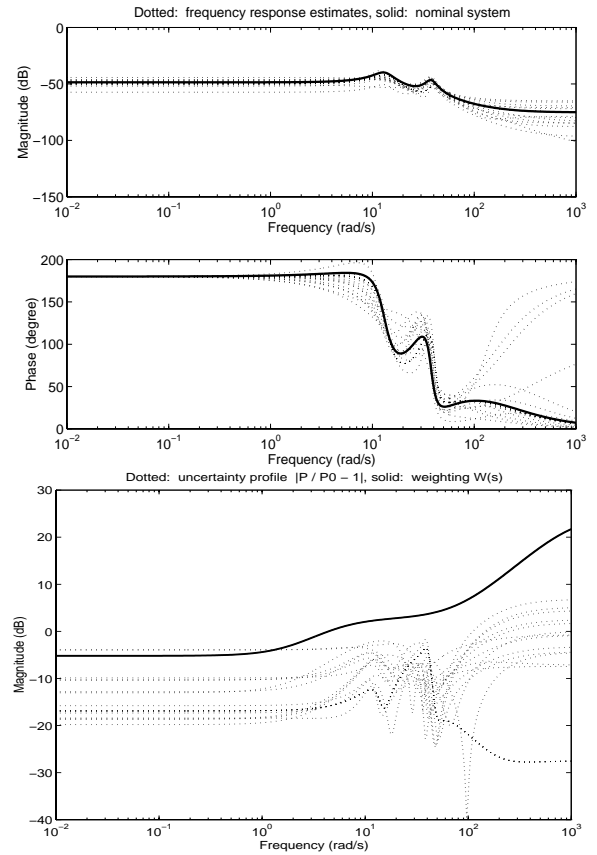


Fig. 4. From top to bottom: (a) Frequency responses of the estimated and nominal systems (top) and (b) the uncertainty profile and the uncertainty weighting function (b)

are depicted in Figure 4b. For best fulfillment of performance requirements which are mainly influenced by the low-frequency characteristics and to avoid conservatism in the control design, the selected uncertainty weighting function falls a little lower than the uncertainty level over low frequencies.

B. Robust H_∞ Control

The H_∞ controller must internally stabilize the closed-loop system, reject the disturbances and increase the damping of the system dominant oscillatory mode as much as possible while the control effort is limited. The block diagram shown in Figure 5 formulates the above-mentioned problem as a standard H_∞ problem. The *generalized regulator problem* is defined as finding a controller $C(s)$ such that:

- $T_{y_1 u_1}$ is internally stable
- $\|T_{y_1 u_1}\|_\infty$ is small

This problem is equivalent to the so-called mixed-sensitivity problem:

$$\min_C \left\| \begin{pmatrix} W_1 W_d C S \\ W_2 W_d T \\ W_3 W_d S \end{pmatrix} \right\|_\infty \quad (5)$$

The weighting functions in Equation (5) have to be appropriately shaped for best fulfillment of the control

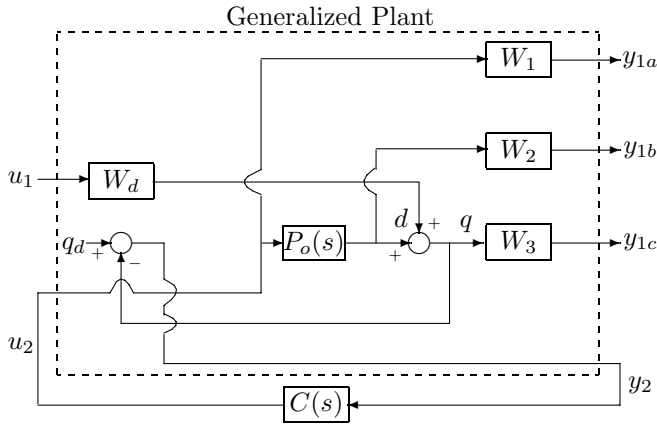


Fig. 5. Closed-loop system as a generalized regulator problem

objectives. To satisfy the primary closed-loop requirement, namely fast settling of the cart, the controller must increase the damping of the system oscillatory modes. The following weight W_d replaces the dominant oscillatory modes of the nominal system at $-2.7 \pm j12.9$ with more stable ones at $-10 \pm j12.9$:

$$W_d(s) = \frac{(s - (-10 + j12.9))(s - (-10 - j12.9))}{(s - (-2.7 + j12.9))(s - (-2.7 - j12.9))}.$$

Choosing $W_2 = W/W_d$, where W is the uncertainty weighting of Equation (4), ensures closed-loop robust stability as $\|WT\|_\infty < 1$. To avoid actuator saturation, weight W_1 should be used to penalize the control effort. Furthermore, W_1W_d should form a band-stop filter to allow maximum control effort around the system dominant oscillatory mode:

$$W_1(s) = 0.15 \frac{(s^2 + 2.4s + 8^2)(s^2 + 4.2s + 14^2)}{(\frac{s}{1.4} + 8)^2(\frac{s}{0.7} + 14)^2} \times \frac{1}{W_d(s)}$$

For simplicity, W_3 which reflects the disturbance rejection properties of the closed-loop system is chosen to be a constant, $W_3 = 0.17$.

Satisfaction of the performance requirements by the consequent H_∞ controller is limited in practice. To explore the reason, closed-loop simulations based on the estimated system (Table 1c) and the designed H_∞ controller are set up. It becomes evident that what limits the degree of performance satisfaction is the motor deadzone due to stiction. The stiction is actually blocking the arm motions for motor currents up to half of its maximum value. Indeed, as shown in Figure 6, the robust H_∞ controller manages to enforce the fast settling of the cart in the absence of motor deadzone, while is not entirely successful in the presence of deadzone. According to this simulation study, the robust control design is entirely successful in satisfying the required control objectives with a limited control effort.

VI. CONCLUSIONS

The RTAC benchmark problem investigates the utility of a rotational proof mass actuator for stabilizing translational motion. In this paper, system parameters were

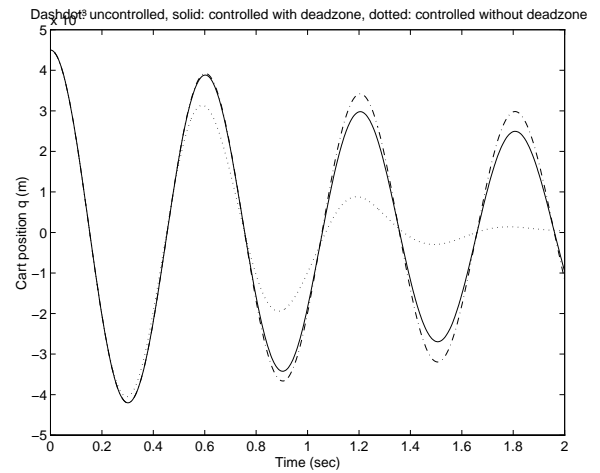


Fig. 6. Free responses of open-loop system (dash-dotted), closed-loop system with deadzone (solid) and closed-loop system without deadzone (dotted)

estimated in a least-squares framework based on free- and forced-oscillation identification experiments. On the other hand, the control requirements fit the robust control synthesis framework. A time-domain nonparametric identification method was used by which the nonlinear system was modelled as a nominal system plus uncertainty. It was confirmed in practice that the deviations of the disturbed nonlinear system from a linear system can successfully be condensed into a small perturbation block. Next, an effective mixed-sensitivity problem was developed to satisfy all performance requirements as well as robust stability despite actuator saturation. Simulation results exhibit the success and effectiveness of the designed robust H_∞ controller.

REFERENCES

- [1] R. J. Kinsey, D. L. Mingori, and R. H. Rand, "Nonlinear Controller to Reduce Resonance Effects of a Dual-Spin Spacecraft through Precession Phase Lock," in *Proceedings of the 31st Conference on Decision and Control*, 1992, pp. 3025–30.
- [2] R. T. Bupp, D. S. Bernestein, and V. T. Coppola, "A Benchmark Problem for Nonlinear Control Design: Problem Statement, Experimental Testbed, and Passive Nonlinear Compensation," in *Proceedings of American Control Conference*, 1995, pp. 4363–7.
- [3] D. K. Linder, T. P. Celano, and E. N. Ide, "Vibration Suppression Using a Proofmass Actuator Operating in Stroke/Force Saturation," *Journal of Vibrations and Control*, vol. 113, pp. 423–33, 1991.
- [4] R. T. Bupp, D. S. Bernestein, and V. T. Coppola, "Experimental Implementation of Integrator Backstepping and Passive Nonlinear Controllers on the RTAC Testbed," in *Proceedings of the IEEE International Conference on Control Applications*, 1996, pp. 279–84.
- [5] W. M. Haddad and V.-S. Chellaboina, "Nonlinear Fixed-Order Dynamic Compensation for Passive Systems," *International Journal of Robust and Nonlinear Control*, vol. 8, no. 4-5, pp. 349–65, April 1998.
- [6] S. Dussey and L. El-Ghaoui, "Measurement Scheduled Control for the RTAC Problem: an LMI Approach," *International Journal of Robust and Nonlinear Control*, vol. 8, no. 4-5, pp. 377–400, April 1998.
- [7] T. Soderstrom and P. Stoica, *System Identification*. Prentice Hall International Ltd, 1989.
- [8] I. Kollar, *Frequency Domain System Identification Toolbox*. The MathWorks Inc., 1994.